PHYSICAL REVIEW B **87**, 174502 (2013)

Evidence of multiband behavior in the superconducting alloy $Zr_{0.96}V_{0.04}B_2$

S. T. Renosto,[1,*] H. Consoline,[1] C. A. M. dos Santos,[1] J. Albino Aguiar,[2] Soon-Gil Jung,[3] J. Vanacken,[3] V. V. Moshchalkov,[3] Z. Fisk,[4] and A. J. S. Machado[1]

[1]*Escola de Engenharia de Lorena, Universidade de São Paulo, P.O. Box 116, Lorena, SP, Brazil*

[2]*Departamento de Física, Universidade Federal de Pernambuco, 50670-901, Recife, PE, Brazil*

[3]*Institute for Nanoscale Physics and Chemistry, K. U. Leuven Celest. 200 D, B-3001 Leuven, Belgium*

[4]*Department of Physics and Astronomy, University of California at Irvine, Irvine, California 92697, USA*

(Received 7 February 2013; revised manuscript received 11 April 2013; published 6 May 2013)

ZrB_2 is a nonsuperconducting Pauli paramagnetic crystallizing in the AlB_2 structure. V substitution for Zr in $Zr_{1-x}V_xB_2$ ($0.01 \leqslant x \leqslant 0.1$) at the few percentage level induces superconductivity with critical temperature reaching a maximum of 8.7 K for $Zr_{0.96}V_{0.04}B_2$ near the solid solubility limit. Specific-heat and lower critical field temperature dependence results suggest the possibility of unconventional superconductivity possibly arising from multiband effects.

DOI: 10.1103/PhysRevB.87.174502 PACS number(s): 74.70.Dd

I. INTRODUCTION

The first superconductors found in the AlB_2 structure were off-stoichiometry NbB_2 and MoB_2 with a respective T_c of 3.87 and 7.45 K.[1] NbB_2 has a wide boron stoichiometry range, its excess B stoichiometry presumably arising from a defect structure. A recent systematic study of Nunes *et al*. of the B-solubility in NbB_2, where the homogeneity of the phases obtained was determined by neutron diffraction, confirmed the maximum critical temperature of 3.9 K.[2] This study raises again the question of the nature of defects in these compounds. NbB_2 spans a wide range of composition as shown in the diagram in Fig. 1.[3]

It appears that the Nb-B interatomic distance in NbB_2 across its stoichiometric range remains constant at 2.43 Å. A superstructure of vacancy defects in the crystal lattice has been proposed to explain the wide stability range of NbB_2.[4] This defect structure is based on a balance of the cohesive forces in the B layers and the expansive forces in the Nb layers. Certainly this defect structure strongly influences the electronic structure, making it highly dependent on stoichiometry.

The discovery of superconductivity in MgB_2 with superconducting critical temperature close to 40 K[5] has renewed interest in AlB_2 structure materials, particularly as candidates for multiband superconductivity. MoB_2 was reviewed by Muzzy *et al*. who reported a systematic study of the substitution of Mo by Zr in the $(Mo_{0.96}Zr_{0.04})_{0.88}B_2$ where the AlB_2 structure is stabilized and superconductivity can exist with critical temperature between 5.9 and 8.2 K.[6] These authors claim that the superconductivity is strongly dependent on a specific defect structure similar to the one that occurs in NbB_2. Another interesting case is $CaSi_2$, which at 15 GPa undergoes an allotropic transformation into the AlB_2 structure with a superconducting critical temperature close to 14.0 K.[7] Although many metal diborides can crystallize in the AlB_2-type structure, superconductivity in this class of material is relatively rare. Theoretical studies suggest that some member compounds are good candidates to exhibit a high superconducting critical temperature. Among these suggested compounds are AuB_2, AgB_2, LiB_2, ZnB_2, and CaB_2.[8–12] However, these theoretical predictions have not been confirmed, and some of the suggested compounds do not exist in the equilibrium phase diagram, for example, ZnB_2, which does not exist on the Zn-B thermodynamic equilibrium binary system. In the binary Zn-B system no solubility exists between Zn and B atoms, and no intermetallic phase is observed. In our opinion the most important criterion for superconductivity in the AlB_2-type structure is defect creation such as occurs in NbB_2. Superconductivity was reported in ZrB_2 with superconducting critical temperature close to 5.5 K.[13] However, this surprising result was not confirmed by other groups. In fact, single crystals of this compound (ZrB_2) are not superconducting.[14] The Zr-B phase diagram suggests that contamination with ZrB_{12}, a known superconductor with critical temperature 5.94 K.[15] ZrB_2, also was studied to high pressure (50 GPa) and no superconductivity was observed.[16]

In this work we present a systematic study of substitution of Zr for V in $Zr_{1-x}V_xB_2$ ($0 \leqslant x \leqslant 1.0$) and find that superconductivity emerge in the nonsuperconductor ZrB_2 matrix for a small content of V, an example where an extremely stressed lattice of the AlB_2 prototype yields superconductivity while the matrix compound is nonsuperconducting. The specific-heat results reveal unambiguously that the $Zr_{0.96}V_{0.04}B_2$ composition is a bulk superconductor with critical temperature close to 8.7 K. Our results suggest that at the limit of stability of the V-doped ZrB_2 the superconducting critical temperature is optimized.

II. EXPERIMENTAL

Polycrystalline $Zr_{1-x}V_xB_2$ samples were prepared from high-purity elements with x values of 0.01, 0.02, 0.03, 0.04, 0.05, 0.07, 0.09, 0.1, and 0.2. The constituent elements were melted in an arc furnace on a water-cooled Cu hearth with Ti getter under high-purity argon. The samples were flipped and remelted five times to ensure good homogeneity. Due to low vapor pressures of the constituent elements at their melting temperatures, the weight losses during arc melting were negligible ($\leqslant 0.5\%$). For the microstructural studies, the samples were prepared by means of hot embedding in resin. The mounted samples were polished with 400–4000 grit sandpaper and subsequently polished with a colloidal silica

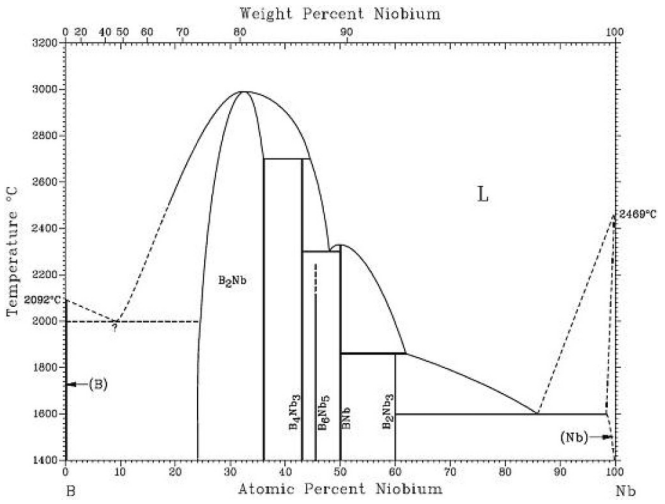

FIG. 1. Phase diagram of the Nb-B system showing the wide solubility range of the NbB_2 phase. Adapted from Ref. 3.

suspension. In order to verify the evolution of the samples with different compositions, the microstructures were analyzed in a scanning electron microscopy (SEM) Hitachi TM 3000, coupled with an Oxford energy dispersive spectrometer (EDS). The SEM micrographs were obtained using the backscattered electron detector for qualitative compositional analyses. All the compositions were characterized by x-ray powder diffractometry (XRD) in a Panalitycal diffractometer (model Empyrean) with detector PIXcel^{3D} using CuKα radiation. The simulation of the structure and refinement of the lattice parameters were obtained using the Rietveld method, adopting as a reference the ZrB_2 phase crystallographic data reported in the literature.[17]

Magnetic, electric, and thermal initial characterizations were made using a Quantum Design PPMS Evercool II. Magnetization (M) measurements were obtained with a vibrating sample measurement system in a DC external field at 50 Oe with both zero field cooling and field cooling regimes, in the temperature (T) range from 2 to 20 K. The hysteresis loops of the M versus applied magnetic field (H) curves were obtained at 2 K in the range $-500 \leqslant \mu_0 H \leqslant 500$ Oe. Electrical transport measurements were done using the conventional four-point method, with a probe current of 1000 μA. The superconducting critical temperature (T_c) was defined as the transition midpoint. The electrical resistivity (ρ) versus T curve was obtained in the temperature range from 2.0 to 300 K. The magnetoresistance was obtained for an applied magnetic field in the range $0 \leqslant \mu_0 H \leqslant 11.5$ T. The specific heat of a piece of material cut from the sample was measured in the range 2.0–10.0 K with a calorimeter in PPMS Evercool II (Quantum Design) using the relaxation method.

III. RESULTS AND DISCUSSION

Figure 2 shows the diffractometry pattern sequence of arc-melted $Zr_{1-x}V_xB_2$ samples with x from 0.01 to 0.1. All reflections can be indexed as an AlB_2 structure (see inset of Fig. 2), space group $P6/mmm$, where the Zr atoms occupy the $1a$ (0,0,0) positions and B atoms the $2d$ (1/3,2/3,1/2). Indeed, the lattice parameters as a function of V content reveal a small

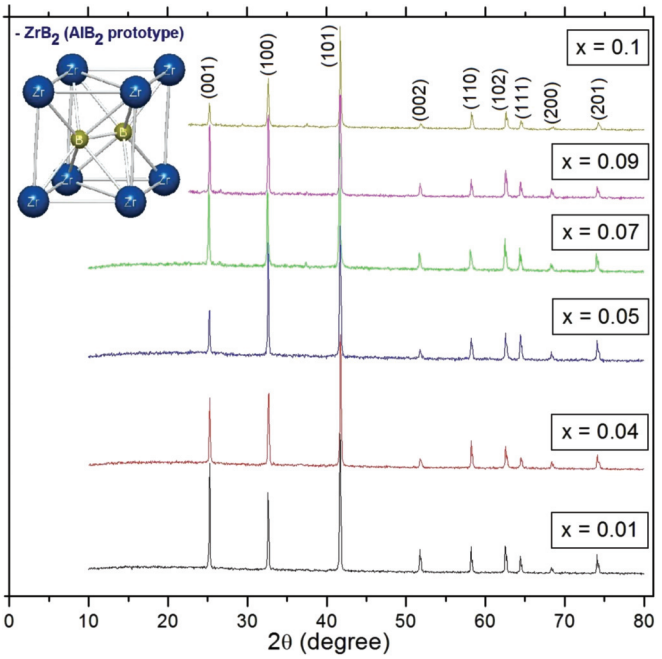

FIG. 2. (Color online) X-ray diffraction pattern for the polycrystalline samples $Zr_{1-x}V_xB_2$ ($0 \leqslant x \leqslant 0.1$). In the inset a AlB_2 structure unit cell is shown, where the blue spheres represent Zr atoms and yellow the B atoms.

but consistent variation, indicating that the $\bar{c}$ lattice parameter systematically decreases with the substitution of Zr for V as shown in Fig. 3. However, the $\bar{a}$ lattice parameter is essentially constant as a function of V content. These results are consistent with the metallic radius of V relative to Zr and indicates that V occupies the positions (0,0,0). A careful analysis of the behavior of the $\bar{c}$ lattice parameters suggests that the solubility limit is low, lower than $x = 0.05$. In the XRD measurements of the samples with composition $x \geqslant 0.7$, a very small segregation of a secondary phase (VB) was observed.

The substitution of Zr by V yields a contraction in the Zr layers in the AlB_2 prototype structure. This is expected since $\bar{a}$ and $\bar{c}$ parameters are approximately 5% and 16% smaller in VB_2 compared to those of ZrB_2. Indeed, VB_2 has $\bar{a} \sim 3.0$ Å and $\bar{c} \sim 3.05$ Å, while ZrB_2 has $\bar{a} \sim 3.16$ Å and $\bar{c} \sim 3.53$ Å.

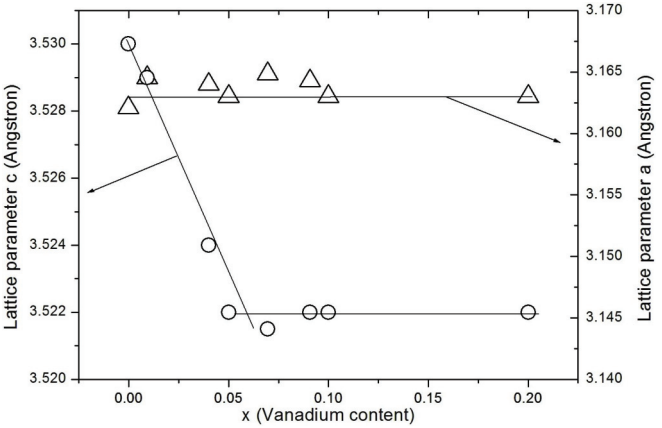

FIG. 3. V compositional dependence of the $\bar{a}$ and $\bar{c}$ lattice parameters for the polycrystalline samples $Zr_{1-x}V_xB_2$ ($0 \leqslant x \leqslant 0.2$).

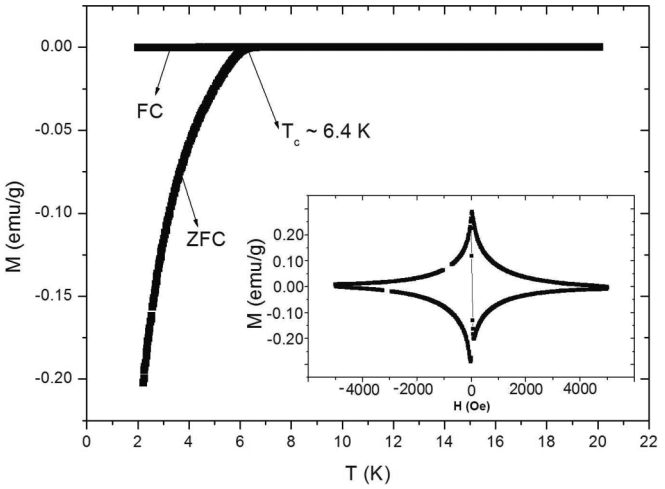

FIG. 4. Temperature dependence of the magnetization for the polycrystalline sample $Zr_{0.99}V_{0.01}B_2$. In the inset, M vs H curve at $T = 2$ K.

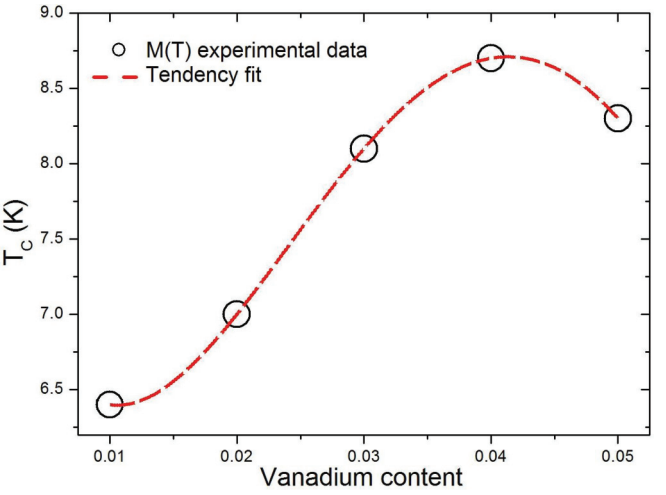

FIG. 6. (Color online) V compositional dependence of the T_c for the polycrystalline samples $Zr_{1-x}V_xB_2$ ($0 \leqslant x \leqslant 0.05$). The dashed line is a guide for the eyes.

These differences explain the larger variation observed for the $\bar{c}$ lattice parameter compared to that of the $\bar{a}$ lattice parameter. The contraction in the lattice parameters occurs until $x \sim 0.05$ in composition, indicating a very limited solubility.

The temperature dependence of the magnetization is shown in Fig. 4. One observes that a superconducting transition emerges even at very low substitution of Zr by V at 6.4 K ($x = 0.01$). In the inset, the M vs H curve at 2 K, characteristic type II superconducting behavior is seen.

These results are especially interesting because they suggest that the V can radically affects the electronic structure of ZrB_2, inducing superconductivity in the nonsuperconducting matrix. Indeed for $x = 0.04$ the superconducting critical temperature reaches the maximum value close to 8.7 K as shown in Fig. 5. The dependence of magnetization with the applied magnetic field at 2.0 K is shown as typical type II behavior in the inset of this figure. For compositions higher than $x = 0.04$ the critical temperature decreases slightly, consistent with the solubility limit. For example, the composition $Zr_{0.95}V_{0.05}B_2$ sample, T_c is close to 8.2 K. Figure 6 shows the dependence of the critical temperature on the function of V content up to the solubility limit. In samples beyond $x = 0.05$ the critical temperature remains at 8.2 K. $M(T)$ measurements show that the critical temperature does not change with higher V content, but the normalized magnetic moment value (emu/g) at 2 K is reduced, suggesting a decrease of the superconducting fraction and consistent with the appearance of a secondary phase. Thus, these results find the optimal level for superconductivity for $Zr_{0.96}V_{0.04}B_2$.

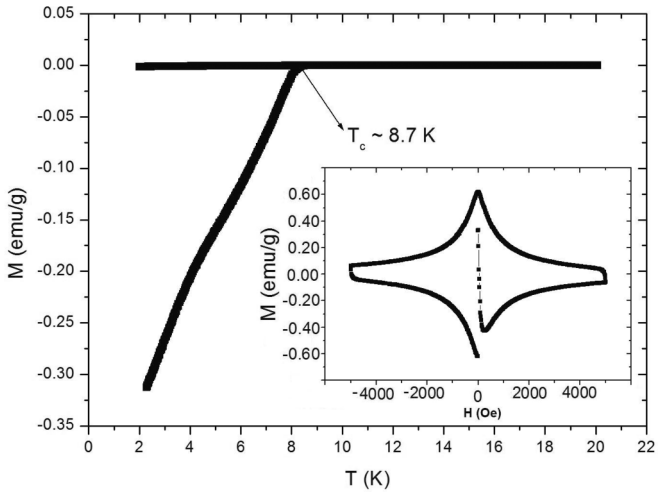

FIG. 5. Temperature dependence of the magnetization for the polycrystalline sample $Zr_{0.96}V_{0.04}B_2$. In the inset, M vs H curve at $T = 2$ K.

Figure 7 shows a SEM micrograph for compositions $x = 0.04$ (a) and 0.05 (b), obtained using the same magnification (300×). It is observed that the microstructure of the $x = 0.04$ sample is uniform and is constituted of a single phase. Indeed, the EDS analysis reveals that the $x = 0.04$ nominal composition is preserved in all grains. However, at $x = 0.05$ a very small segregation can be observed in the grain boundary; this is consistent with the lattice parameter analysis. The difference of grain size in the $x = 0.04$ (a) and 0.05 (b) samples can be explained by Zener pinning effects, where the small segregation acts as a barrier in the grain

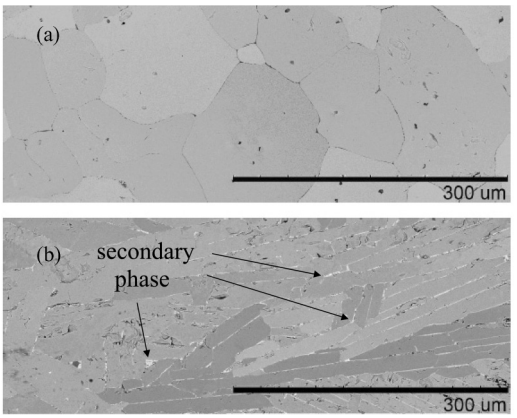

FIG. 7. SEM micrograph of the (a) $Zr_{0.96}V_{0.04}B_2$ and (b) $Zr_{0.95}V_{0.05}B_2$ samples.

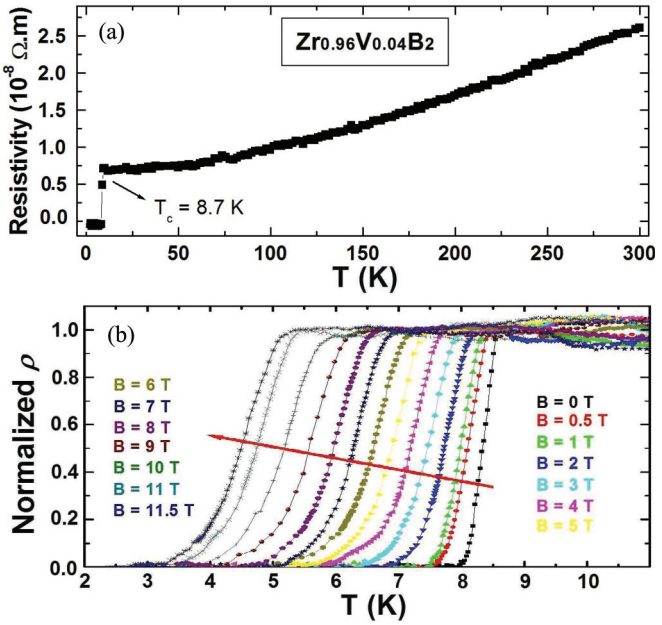

FIG. 8. (Color online) Temperature dependence of the (a) resistivity and (b) normalized resistivity with an applied field, for the $Zr_{0.96}V_{0.04}B_2$ sample.

boundary motion. Since the $Zr_{0.96}V_{0.04}B_2$ sample presents the highest superconducting temperature, we will discuss in more detail this composition. The temperature dependence of the resistivity for the $Zr_{0.96}V_{0.04}B_2$ sample is shown in Fig. 8. A sharp resistivity transition close to 8.7 K (onset temperature) is clearly observed in Fig. 8(a), indicative of the good quality of the sample. This result is consistent with magnetization results displayed in Fig. 5. The temperature dependence of the normalized resistivity obtained for an applied magnetic field in the range $0 \leqslant \mu_0 H \leqslant 11.5$ T is shown in Fig. 8(b). These results suggest that the upper critical field is quite high since even in an applied magnetic field of $\mu_0 H = 11.5$ T the material is still superconducting with critical temperature close to 4.5 K. A estimate of the upper critical field in 0 K $[\mu_0 H_{c2}(0)]$ can be made through the Werthamer, Helfand, and Hohenberg (WHH) formula,[18] in the limit of a short electronic mean-free path (dirty limit) given by

$$\mu_0 H_{c2}(0) = -0.693 T_c (dH_{c2}/dT)_{T=Tc} \quad (1)$$

The temperature dependence of the upper critical field $[\mu_0 H_{c2}(T)]$ is shown in Fig. 9 where the red line represents the conventional fitting with $\mu_0 H_{c2}(0)$ obtained using the WHH formula [Eq. (1)]. The $\mu_0 H_{c2}(0)$ is estimated to be ~16.3 T, a surprisingly high upper critical field for this class of the material.[19] The fitting in Fig. 9 data allows an estimation of the coherence length through of the Ginzburg-Landau formula:

$$\mu_0 H_{c2}(0) = \phi_0 / 2\pi \xi_0^2, \quad (2)$$

where ϕ_0 is a quantum flux equal 2.068×10^{-15} T m^{-2}, which yields $\xi_0 \sim 4.49$ nm at 0 K. All these results are consistent with bulk superconductivity in $Zr_{0.96}V_{0.04}B_2$.

The lower critical field (H_{c1}) can be estimated from the applied magnetic field dependence of the magnetization at several temperatures shown in Fig. 10(a), which gives $\mu_0 H_{c1}(0) \sim$ 2.5 mT. The values of H_{c1} were determined by examining the

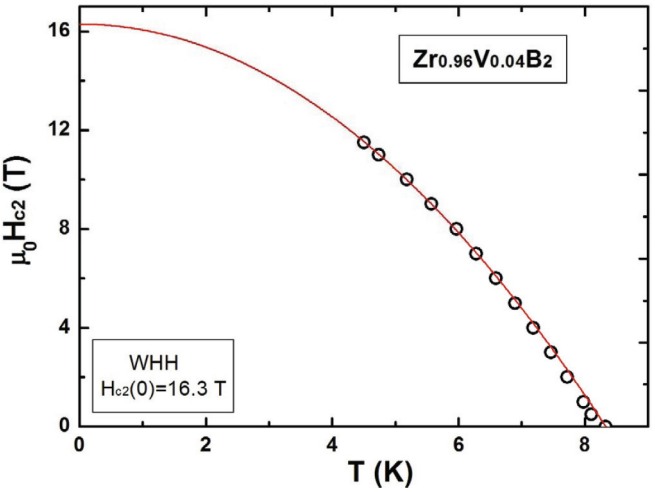

FIG. 9. (Color online) The temperature dependence of the $\mu_0 H_{c2}$ for the $Zr_{0.96}V_{0.04}B_2$ sample. The continuous line was obtained by conventional fitting: $\mu_0 H_{c2}(T) = \mu_0 H_{c2}(0)[1-(T/T_c)^2]$.

point of departure from linearity on the slope of the magnetization curve, using the criterion of $\Delta M = 10^{-3}$ emu for the difference between the Meissner line and magnetization signal,[20] as is shown in Fig. 10(b). However, the dependence of the H_{c1} with the reduced temperature ($t = T/T_c$) reveals a negative curvature suggesting unconventional behavior (see Fig. 11).

This kind of the unconventional behavior in $H_{c1}(t)$ can be observed in materials which are considered multiband compounds.[18,20,21] The deviation is also observed in MgB_2, which is a superconductor with two bands arising from the holelike boron σ band and the π band.[9,22] Hence, the two-band Eliashberg theory is generally taken as the appropriate description rather than the isotropic single band model.[23,24]

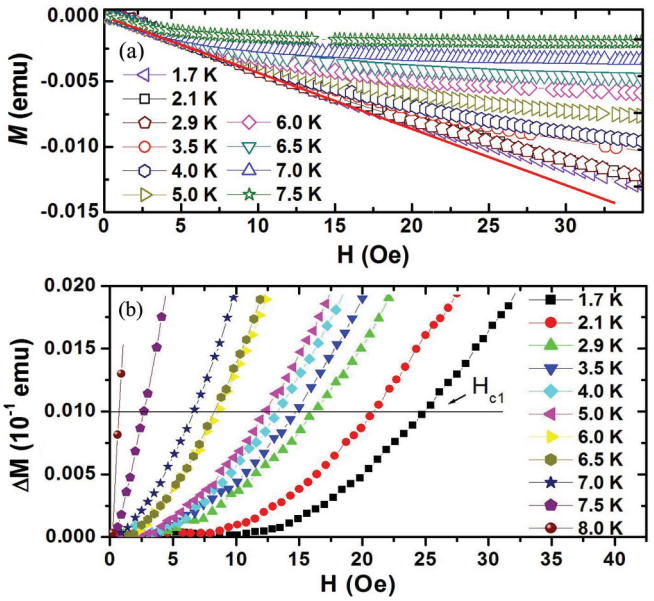

FIG. 10. (Color online) (a) Magnetization versus applied field at several temperatures, for the $Zr_{0.96}V_{0.04}B_2$ sample. The red line represents the Meissner line. (b) ΔM vs H, which plots the difference between the Meissner line and the $M(H)$ curve. The H_{c1} was determined by using the criterion of $\Delta M = 10^{-3}$ emu.

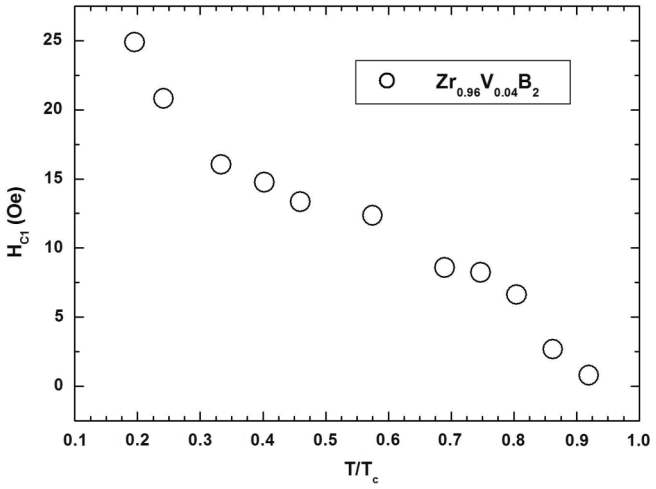

FIG. 11. Reduced temperature dependence of the H_{c1} for the $Zr_{0.96}V_{0.04}B_2$ sample.

The TB Eliashberg model was applied for determining the behavior of H_{c2} in YNi_2B_2C and $LuNi_2B_2C$, and MgB_2.[23,25] The temperature dependence of the upper critical field present an upward curvature, provided by electrons at distinctly bands. This can be explained by (i) significantly different Fermi velocities (V_F) at the two bands and (ii) strong coupling in the small-V_F band and sizable coupling between the small-V_F and large-V_F bands, where V_F is the Fermi velocity. This upward curvature will increase as the ratio of the Fermi velocities increases.[26] In contrast, when the strongest coupling is in the large-V_F band the curvature of $H_{c2}(T)$ near T_c is negative.[27,28] Thus the result presented in Fig. 9 can be interpreted as the average of the contribution of two coupled superconductors, one with a small $H_c(0)$ and high T_c and the other with large $H_{c2}(T)$ and small T_c. This scenario would explain the apparent contradiction between the temperature dependence of $H_{c1}(T)$ and $H_{c2}(T)$ seen in Figs. 11 and 9, respectively. To really

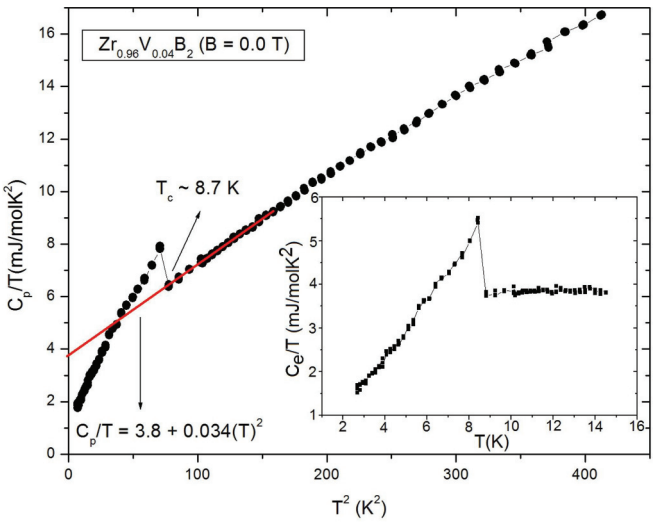

FIG. 12. (Color online) Temperature dependence of the C_P for the $Zr_{0.96}V_{0.04}B_2$ sample. In the inset the electronic contribution of the C_P. The continuous line is the fitting based on the normal state contribution.

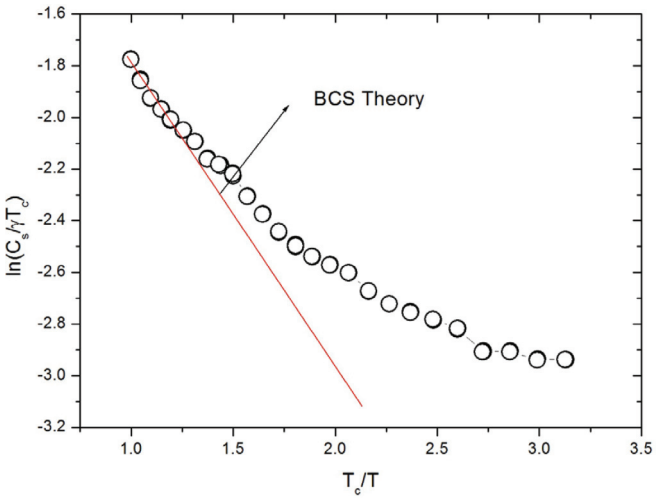

FIG. 13. (Color online) Linearized superconducting contribution to the C_P [$\ln(C_s/\gamma T_c)$], as a function of T_c/T for the $Zr_{0.96}V_{0.04}B_2$ sample. The continuous line is a fitting based on the BCS theory.

clarify this point measurements in single crystals are needed. Borrowing this reasoning we speculate that $Zr_{0.96}V_{0.04}B_2$ could be a further example of a multiband in the same MgB_2 prototype structure.

In order to further confirm the bulk superconductivity of polycrystalline $Zr_{0.96}V_{0.04}B_2$ sample we measured the zero applied magnetic field temperature dependence of the specific-heat (C_P). An anomaly (jump) at 8.7 K is clearly observed in the Cp/T vs T^2 measurement as shown in Fig. 12. This result is totally consistent with the M vs T and ρ vs T measurements where the same superconducting critical temperature is seen. The normal state can be fitted to the expression $C_p = \gamma T + \beta T^3$ by a least-square analysis, which yields the value $\gamma = 3.8$ (mJ/molK^2) and $\beta = 0.034$ (mJ/molK^4). The β value corresponding to Debye temperature $\Theta_D \sim 555.6$ K, and the electronic coefficient (γ is the Sommerfeld constant) measures the density of the states at the Fermi level. The subtraction of the phonon contribution allows us to isolate the electronic contribution to the specific heat, which can be plotted as C_s/T vs T as shown in the inset of this figure. These results show that $Zr_{0.96}V_{0.04}B_2$ is unambiguously a bulk superconducting material. However, the size of the jump ($\Delta C/\gamma T_c$) is about 0.42, which is considerably smaller than the weak coupling BCS prediction (1.43). This value suggests that the superconductivity in this material could be unconventional in its origin. In fact, the $\ln(C_s/\gamma T_c)$ against T_c/T displays a strong divergence from BCS theory already close to T_c (see Fig. 13), which is consistent with the unconventional behavior,[29] as observed in the jump shown in the inset of the Fig. 12.

The origin of the unconventional behavior observed in H_{c1} and in specific heat is not obvious but could be related to the multiband characteristic of this kind of the structure (σ and π bands), which seems to be typical of the AlB_2 prototype structure.

IV. CONCLUSIONS

In this paper we have presented a systematic study of $Zr_{1-x}V_xB_2$ polycrystalline samples. Our results show

that vanadium is able to induce superconductivity in the nonsuperconductor material ZrB_2. The excellent agreement of transition temperature as characterized by the magnetic, resistivity, and specific-heat data unambiguously indicates that the $Zr_{0.96}V_{0.04}B_2$ compound exhibits a bulk superconducting transition temperature ~8.7 K. Unconventional superconductivity related to multiple bands at the Fermi surface is suggested as a possibility for our findings.

ACKNOWLEDGMENTS

This work was financed by the Brazilian agencies CAPES, CNPq, FACEPE (APQ-0589-1.05-08), and FAPESP (2009/54001-2, 2010/11770-3, and 2011/05961-3) and the Brazilian- Belgium cooperation project CNPq-FWO, under CNPq Grants No. 490297/2009-9 and No. 302892/2011-7. Z.F. is supported by AFOSR MURI.

*renosto@usp.br

[1] A. S. Cooper, E. Corenzwit, L. D. Longinotti, B. T. Matthias, and W. H. Zachariasen, Proc. Natl. Acad. Sci. USA **67**, 313Y (1970).

[2] C. A. Nunes, D. Kaczorowski, P. Rogle, M. R. Baldissera, P. A. Suzuki, G. C. Coelho, A. Grytsiv, G. André, F. Bouree, and S. Okada, Acta Mater. **53**, 3679 (2005).

[3] T. Massalski. H. Okomono, P. Subramanian, and L. Kacprozak, *Binary Alloy Phase Diagrams*, 2nd ed. (American Society for Metals, Metals Park, 1990).

[4] G. A. Meerson and G. V. Samsonov, Zh. Prikl. Khim. **27**, 1053 (1954) [J. Appl. Chem. USSR **27**, 1053 (1954)].

[5] J. Nagamatsu, N. Nakagawa, Y. Z. Murakana, and J. Akimitsu, Nature (London) **410**, 63 (2001).

[6] L. E. Muzzy, M. Avdeev, G. Lawes, M. K. Haas, H. W. Zandbergen, A. P. Ramirez, J. D. Jorgensen, and R. J. Cava, Physica C **382**, 153 (2002).

[7] S. Sanfilippo, H. Elsinger, M. Nunez-Regueiro, O. Laborde, S. LeFloch, M. Affronte, G. L. Olcese, and A. Palenzona, Phys. Rev. B **61**, R3800 (2000).

[8] A. L. Ivanovski, Usp. Khim. **70**, 811 (2001).

[9] J. Kortus, I. I. Mazin, K. D. Belashchenko, V. P. Antropov, and L. L. Boyer, Phys. Rev. Lett. **86**, 4656 (2001).

[10] J. M. An and W. E. Pickett, Phys. Rev. Lett. **86**, 4366 (2001).

[11] N. I. Medvedeva, A. L. Ivanovskii, J. E. Medvedeva, and A. J. Freeman, Phys. Rev. B **64**, 020502 (2001).

[12] I. R. Shein and A. L. Ivanovskii, Phys. Solid State **44**, 1833 (2002).

[13] V. A. Gasparov, N. S. Sidorov, I. I. Zver'kova, and M. P. Kulakov, JETP Lett. **73**, 532 (2001).

[14] V. A. Gasparov, N. S. Sidorov, and I. I. Zverkova, Phys. Rev. B **73**, 094510 (2006).

[15] Z. Fisk, A. C. Lawson, B. T. Matthias, and E. Corenzwit, Phys. Lett. A **37**, 251 (1971).

[16] A. S. Pereira, C. A. Perottoni, J. A. H. da Jornada, J. M. Leger, and J. Haines, J. Phys.: Condens. Matter **14**, 10615 (2002).

[17] W. G. Fahrenholtz and G. E. Hilmas, J. Am. Ceram. Soc. **90**, 1347 (2007).

[18] N. R. Werthamer, E. Helfand, and P. C. Hohenberg, Phys. Rev. **147**, 295 (1966).

[19] M. Mudgel, V. P. S. Awana, H. Kishan, I. Felner, G. A. Alvarez, and G. L. Bhalla, J. Appl. Phys. **105**, 07E313 (2009).

[20] S. L. Li, H. H. Wen, Z. W. Zhao, Y. M. Ni, Z. A. Ren, G. C. Che, H. P. Yang, Z. Y. Liu, and Z. X. Zhao, Phys. Rev. B **64**, 094522 (2001).

[21] I. N. Askerzade, A. Gencer, and N. Güçlü, Supercond. Sci. Technol. **15**, L13 (2002).

[22] Y. Kong, O. V. Dolgov, O. Jepsen, and O. K. Andersen, Phys. Rev. B **64**, 020501 (2001).

[23] S. V. Shulga, S. L. Drechsler, G. Fuchs, K. H. Muller, K. Winzer, M. Heinecke, and K. Krug, Phys. Rev. Lett. **80**, 1730 (1998).

[24] J. P. Carbotte, Rev. Mod. Phys. **62**, 1027 (1990).

[25] S. V. Shulga, S. L. Drechsler, H. Eschrig, H. Rosner, and W. Pickett, arXiv:cond-mat/0103154.

[26] M. Mansor and J. P. Carbotte, Phys. Rev. B **72**, 024538 (2005).

[27] P. Entel *et al.*, J. Low Temp. Phys. **22**, 613 (1976).

[28] E. Langmann, Phys. Rev. B **46**, 9104 (1992).

[29] H. J. Choi, D. Roundy, H. Sun, M. L. Cohen, and S. G. Loule, Nature (London) **418**, 758 (2002).